Capture Dense: Markerless Motion Capture Meets Dense Pose Estimation

Xiu Li[1,2] Yebin Liu[1] Hanbyul Joo[2] Qionghai Dai[1] Yaser Sheikh[2]

Tsinghua University[1] Carnegie Mellon University[2]

Abstract

We present a method to combine markerless motion capture and dense pose feature estimation into a single framework. We demonstrate that dense pose information can help for multiview/single-view motion capture, and multiview motion capture can help the collection of high quality dataset for training the dense pose detector. Specifically, we first introduce a novel markerless motion capture method that can take advantage of dense parsing capability provided by the dense pose detector. Thanks to the introduced dense human parsing ability, our method is demonstrated much more efficient, and accurate compared with the available sate-of-the-art markerless motion capture approach. Second, we improve the performance of available dense pose detector by using multiview markerless motion capture data. Such dataset is beneficial to dense pose training because they are more dense and accurate and consistent , and can compensate for the corner cases such as unusual viewpoints. We quantitatively demonstrate the improved performance of our dense pose detector over the available DensePose. Our dense pose dataset and detector will be made public.

1. Introduction

Recently, human parsing in a single view image receives more and more attentions in computer vision and computer graphics. Sparse parsing technique focuses on 2D human skeleton detection [33, 43, 9], and lately lifts to 3D skeleton estimation [41, 29] from a single image. While sparse parsing technique has shown applications in motion capture and analysis [30], the 2D dense human parsing [19, 18] and 3D dense human parsing techniques [4, 7, 23] reveal per-pixel semantic information and can be further applied in human body reconstruction and performance capture [6, 3, 47], image editing and re-enactment [31, 34], therefore a very important and promising direction. The relation between 2D dense parsing (dense pose) and 3D dense parsing is similar to the 2D skeleton detection and 3D skeleton detection. Since the performance of 3D skeleton detection heavily depends on the 2D part [29], 2D dense human parsing will the corner stone for future 3D human reconstructions.

DensePose [18], as the latest proposed and the state-of-the-art 2D dense human parsing technology, has captured many attentions in this field [31]. The success of DensePose relies on a training dataset containing large amount of in-the-wild human images manually annoted by human labor. However, such dataset is limited in accuracy because human annotations are far from real dense feature annotation. In fact, human can only label sparse correspondence features in DensePose. Moreover, there exists large amount of ambiguities for human to understand the real correspondences, especially for the complex rotation of arm regions in the human image, and also corner case images such as images captured from top-down views.

At the other end of spectrum is the markerless human motion capture using multiview video cameras [26, 27]. Given tens or even hundreds of cameras from different viewpoints, the state-of-the-art markerless motion capture method can produce human shape and pose information of body, face, hands and fingers, called TotalCapture [22]. While this is the only available markerless system that can simultaneously produce all of the 3D body elements, the system is still lack in efficiency and accuracy. First, it requires surface point cloud calculation using multiview triangulation for body shape fitting, which is a very time-consuming step and can not guarantee to have good results on challenging surface regions. More importantly, the system relies on 2D sparse parsing technique like OpenPose [2], which only captures joint position information and thus difficult to derive skeleton joint rotation even using multiview skeleton position constrains.

In this paper, we put forward the idea that the puzzle on how to obtain accurate and dense pose and the difficulty on how to achieve more efficient and accurate total motion capture can be tackled as a single problem and can be solved together. On the one hand, dense pose helps total motion capture, since available binocular or multiview triangulation methods only use low-level photometric cues for 3D reconstruction [11, 13], while a high quality dense pose can provide additional high-level semantic cues in stereo

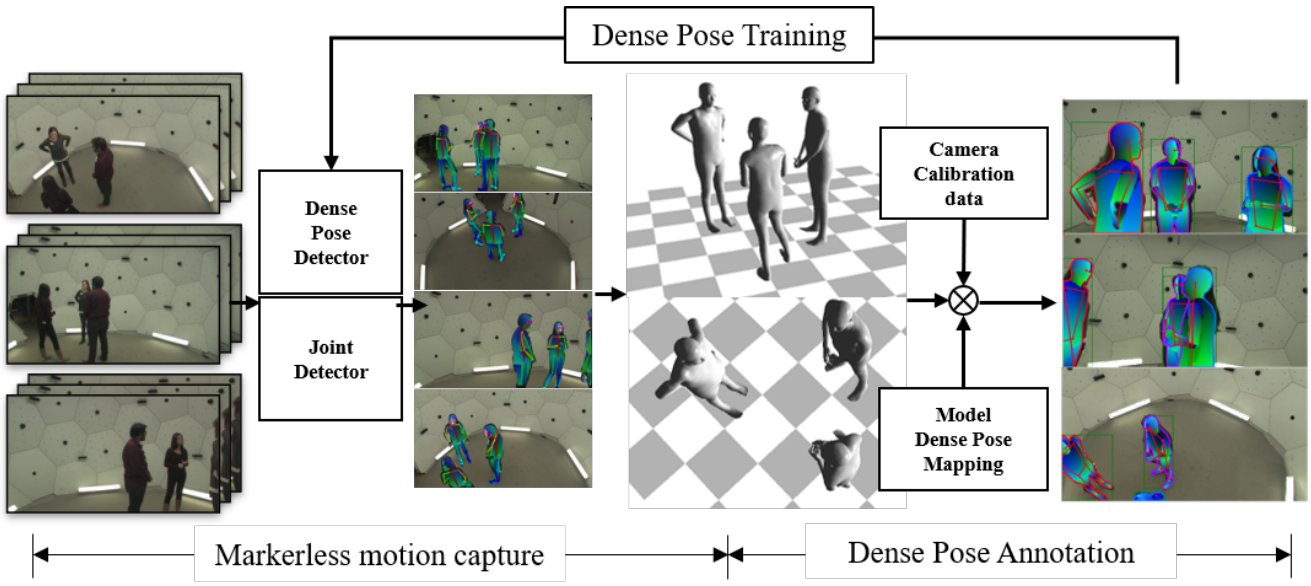

Figure 1. Overview of the pipelines and components of our optimization framework. Three main steps including markerless motion capture, dense pose data annotation, and dense pose tracking. All the three steps in an optimization loop.

matching for better *human shape reconstruction*. Moreover, the dense pose upgrades the traditional sparse feature (2D skeleton) matching to dense feature matching, which contains surface rotation information for better *human pose estimation*. On the other hand, the multiview markerless motion capture environment provides multiview constrains and is able to produce automatic, dense, and highly accurate feature labeling on each input image, corner cases (top-down views), as well as quantitative evaluation mechanism from multiview constraints, which are not shared by the manual annotation.

Based on the above reasoning, our key idea in this paper is to develop an optimization system that can combine markerless motion capture and dense pose estimation into a single framework and make them in an optimization loop. Specifically, dense feature parsing can be beneficial to markerless motion capture and in return, markerless motion capture helps for dense body feature annotation. With this goal, we make the following technique contributions in this paper.

- We propose a learning framework that can combine the generation of dense pose images and the optimization of total motion capture in an optimization loop.
- We propose a two-step markerless motion capture approach, with the second step taking advantage of multiview dense pose parsing to achieve high quality shape and pose reconstruction. Our method is much faster than the state-of-the-art [22], and demonstrates improvements on reconstruction of body part rotations.
- We contribute a method to efficiently generate a large scale of dense pose dataset in practical time and meanwhile guarantee the correctness of the labels, based on the multiview motion capture results. We quantitatively demonstrate the improved performance of our dense pose detector over the available one [18]. Our dense pose dataset and detector will be made public.

2. Related work

In the past two decades, markerless motion capture methods have been explored in computer vision and graphics community. The researches can be categorized into generative methods and discriminative methods. In between, generative methods using a pre-scanned 3D template model with embedded skeleton are most popular and standard [26, 17, 10, 8, 24, 42, 12, 40]. By optimizing the skeleton motion, such that the template model can be deformed accordingly and align with the input images, the skeleton motion can be estimated. Generally, features correspondences between the temporally former tracked model and the current images are necessary. These features correspondences are usually developed by iterative closest point (ICP) method [48], which is not semantically accurate and is easy to trap into local minimum or even fragile when large motion happens. Although depth information can be introduced by using depth cameras [46], the distance closest feature matching is still used, resulting in similar ambiguities.

Statistics deformable body models [28, 36] were introduced to express both shape and body variations of humans. Generative optimization methods [6, 47] using such models have been introduced to remove the requirement for pre-scanned human templates. However, such models

only describes human body under minimum clothing, thus the modeling of clothing and body are required for general clothing peoples in multiview camera setup [35]. Using a single depth camera, DoubleFusion [47] demonstrates the using of SMPL [28] in aiding of fast and robust motion tracking and surface reconstruction. However, this system also relies on ICP-like method for non-rigid surface and skeleton tracking, resulting in only plausible motion accuracy, especially for hand and arm regions.

Discriminative methods parse human skeleton for a single RGB image or depth image. Ganapathi et al. [16] and Shotton et al. [38] have demonstrated realtime performance and enabled enormous applications with a depth camera. Skeleton motion of multiple human bodies can also be track using the discriminative method under static multi-camera setup [5] or even hundreds of RGB cameras [21]. Compared with the generative methods, discriminative methods lack of accuracy and temporal coherence. Hybrid methods combine the strength of discriminative methods and generative methods to improve tracking robustness [44].

Recent advances in 2D human keypoint detection [9, 32, 43] using deep convolutional network make it possible to lift to single image 3D skeleton detection [29, 41, 7, 23], or to reliably reconstruct 3D keypoints in a multiview setup, where a 3D model can be fitted [15, 21]. There are also single view markerless motion capture methods [30, 45] by running generative optimization on the 2D human keypoint detectors. Using hundreds of cameras, it has been demonstrated that shape and pose of torso, hands and face can be well fit to body template by fusing multiview 2D detectors and photometric cues. However, sparse keypoint detectors only give skeleton joint positions, therefore limited in efficiency and accuracy in motion capture accuracy.

Contrary to 2D skeleton detectors, dense human parsing techniques, i.e., dense pose detector [18, 19] are introduced recently by running deep learning on manually label datasets. Dense pose detector provides dense semantic information on the human pixels, thus a more powerful detector for solving skeleton joint rotation and human shape in markerless motion capture. The key idea of this work is most similar to Simon et al. [39]. They demonstrated that multiview image constrain can be help in training 2D hand pose detection. This paper explores how multiview image can aid in training 2D dense pose detector. Overall, our paper distincts with all the former works by introducing dense human parsing technique into multiview markerless shape and motion capture, and make them in a loop. We demonstrate superior performance of our results in both motion capture and dense pose estimation after running our loop optimization.

Method	TotalCapture		Ours	
Stage	Joint	PtCloud Opt	Joint	Refine
Time(s)	60+	120+	0.54	5
mean	85.91%	87.74%	84.17%	87.15%
Std.	4.57	4.18	4.57	4.53

Table 1. Analysis of markerless motion capture performance. Our Capture-Dense system greatly reduce the runtime while keeping comparable results to TotalCapture. (Note also that our performance on body part rotations is visually better than TotalCapture, which is hard to be quantitatively measured.

3. Overview

The final goal of this work is to develop a better dense pose estimator by using multiview markerless motion capture data for data training. Therefore, instead of manually labelling dense pose images, we separate the whole task into three stages, as shown in Fig. 1. Firstly, we use existing skeleton joint detector [2] and dense pose detector [18] to extract feature tracks for the multiview inputs. By multiview triangulation and model fitting on the dense pose and skeleton results, we can capture total human shapes and motions expressed as Adam model sequence, see Sect. 4. In the second stage, we parse the Adam model sequences into dense pose correspondence and render them to generate large-scale dense pose annotations, see Sect. 5. In the third stage, we feed the new dense pose dataset into the dense pose training process to improve the dense pose feature detector. We loop these three stages and run it automatically by feeding the new DensePose detector to markerless motion capture stage.

4. Markeless Motion Capture

In the markerless motion capture stage, we aim at capturing large amount of shape and pose sequences for the later dense pose data generation. Similar to TotalCapture [22], we use the Adam model instead of SMPL model for shape representation of human, because of its total motion describing ability for torso, hands and face for potential further usage[1]. The original Totalcapture pipeline requires the using MVS point cloud estimation [1] for accurate human shape reconstruction, while this is accurate, it is too time-consuming for data generation. Moreover, most of the available markerless Mocap systems including Totalcapture fuse multiview 2D joint feature detectors [2] to get 3D joint positions, followed with the need of leveraging motion priors to regularize and regress for joint rotations. However, in practice it is hard to tune the regularization parameter in the optimization stage. Large prior and regression weights will lead to large joint fitting errors while small prior will lead to

[1]The most recent MANO-SMPL[37] model can also describe body and hand motion

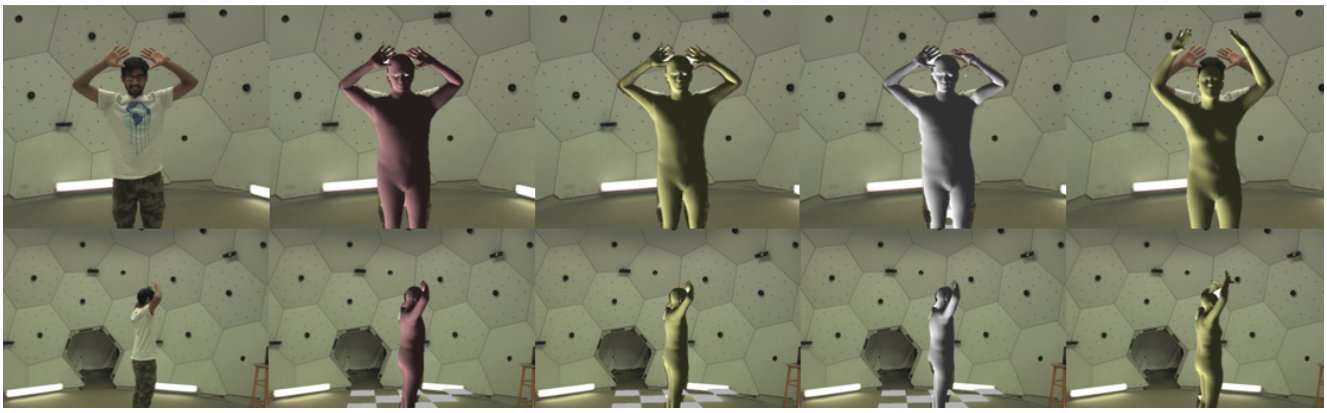

Figure 2. Illustration and comparison of Mocap results. From left to right, one of the input images, our result after shape and pose fitting 4.1, the final refined results 4.2, TotalCapture result [22], result using SMPL model (w/o hands). Note that the shape in our fitting result is not accurate and artifact appeared at the left arm (rotation problem) in the TotalCapture result.

'un-natural' joint rotation even the body joints are perfectly fitted, as shown in Fig. 2.

To this end, we propose a novel markerless motion capture method which takes advantage of the dense pose parsing information, to save the computation time for shape optimization and reduce ambiguity in pose estimation. In the following, given a multi-view image sequences with calibrated camera parameters, we first use the state-of-the-art joint detector [2] to extract multi-view 2D body joint positions to fit for the initial shape and pose parameters 4.1, and then refine the results based on the multi-view dense parsing information 4.2.

4.1. Shape and Pose Fitting

Given the 2D joints locations detected by OpenPose in each view, we first calculate the 3D skeleton positions considering joint association and noise and error removal using method described in [21]. We then fit the target mesh model to 3D joints following a similar method in [22] by minimizing their euclidean distance as

$$\theta, \beta, \mathbf{T} = \arg\min E_{joint} + E_{prior}(\theta, \beta). \tag{1}$$

Here,

$$E_{joint} = \|\mathbf{J}(\theta, \beta, T) - J_t\|, \tag{2}$$

where J_t is the estimated joint positions, and $\mathbf{J}(\cdot)$ is a mapping function maps pose parameter θ, shape parameter β, and global transform T to joint positions as

$$\mathbf{J}^{3P} = \mathcal{J}^{3P\times 3M}\mathbf{V}^{3M}, \tag{3}$$

where $\mathcal{J}^{3P\times 3M}$ is the sparse joint regressor we build for transforming vertices on Adam mesh model to OpenPose joint positions. M is the number of vertices and P is the number of joints.

$$\mathbf{V}^{3N} = \mathbf{T}\mathcal{W}(\theta^{3(P-1)}, \beta^K), \mathbf{T} \in SE(3) \tag{4}$$

where the $\mathcal{W}(\cdot)$ denotes the linear blender skinning [28, 22] which transfer θ, β to a mesh model in local body-centric system.. To get better convergence and reasonable fitting results, we modify the original mean-zeros norm in E_{prior} to anatomical priors as proposed in [7]. The joint angle prior for body is learned from CMU Mocap while the hand prior is learned with from TotalCapture and MANO [37] training data.

4.2. Shape and Pose Refinement

The shape and pose results from above process contains some error since (1) shape parameters can not be fully determined by joint positions only, (2) joint locations from OpenPose is not semantic accurate and stable, as even static human motions can produce jittering detection results, thus the fitted results can not be perfectly aligned with the body and (3) the fitting of fingers is usually noisy, which may lead to wrong arm rotations.

We therefore turn to use dense pose information for pose and shape refinement, since it gives the per-pixel spatially continuous semantic information of human body. Although a single dense pose may not be accurate, the fusion of multi-view dense poses can remove noises and provide dense surface information for forming the shape and pose. Basically, given a human person image, the output of a dense pose detector is an UVI map, with each pixel on the human body a triplet vector (u, v, i) encoding its correspondence to a SMPL model vertex. Here, U and V stand for the barycentric coordinates and I for the index of the segmented body part. In total, there are 24 parts for a human body in dense pose.

Our key idea for shape and pose refinement is to drive the surface vertices on the Adam model (obtained from Sect. 4.1) to align with the multi-view UVI maps, by optimizing the shape and pose parameters. To this end, similar to the traditional ICP based pose optimization [26], we

need to compute correspondence pairs between vertices on the Adam model and pixels on each UVI map. We denote the feature pairs for vertex m and its corresponding feature p_n on image n as (m, p_n), with $n = 1, .., N$ and N is the number of views. The problem now is how we develop the correspondences (m, p_n). In this step, since the UVI map only semantically maps to the SMPL model, we need to build the Adam-UVI map beforehand, which is also required in the data annotation step, see Sect. 5.1 for detail. With this map, each Adam model vertex m will has its own UVI coding value (u_m, v_m, i_m). Then for each model vertex on the Adam model, we project it to each image and search for a best matched pixel in a local neighbourhood with distance threshold ϵ_I. We fetch the pixel p with the minimum euclidean distance $\|u_m - u_p, v_m - v_p\|_2$ as the correspondence to vertex m. Here, we set different thresholds for different parts based on their coverage size on the 3D mesh model. For small body parts, we will up-sample their UVI map to achieve sub-pixel accuracy. Note that this process can be done in a fully parallel framework. We can get up to MN (N is the number of views, and M is the number of vertices on the model) point tracks within several milliseconds. Comparing to conventional photometric-error based multi-view system, the time-consumption and computation-resource usage in this stage can be ignored.

Based on the multi-view correspondence (m, p_n), $n = 1, .., N$, we back project each p_n to the 3D space by running a standard RANSAC-based multi-view triangulation [20] to get 3D position x^m, as the 3D correspondence to vertex m. Finally, we can form a dense pose term by

$$E_{dense} = \sum_{i=1}^{M} \rho_i\left(\frac{\|(\mathbf{v}^m - \mathbf{x}^m\|}{\sigma_i}\right) \tag{5}$$

where $\rho_i(\cdot)$ is the Geman-McClure robust filter and σ_i is the epipolar error for point i. By adding it to Eqn. 1 as

$$\theta, \beta, \mathbf{T} = \arg\min(E_{joint} + E_{prior} + \alpha E_{dense}). \tag{6}$$

We iterate the optimization of the above energy function and the building of correspondences for 4 times. We gradually increasing the weight α in the iterations. Fig. 2 shows the comparison results with and without using the dense pose refinement, and also with TotalCapture and using the basic SMPL model. Our method outperforms the others in pose and shape qualitatively while greatly reduce the run-time.

Using the proposed motion capture pipeline, we have tracked and reconstructed 1.8M Adam model instances. We develop automatic algorithms to detect low quality results by examining how well the Adam model fit with the multi-view image silhouettes and how well the 3D skeleton fit with the detected 2D skeleton. We remove those instances and finally get 1.2M Adam model instances for the building of dense pose dataset. Totally, there are $37M$ image-Adam model correspondences.

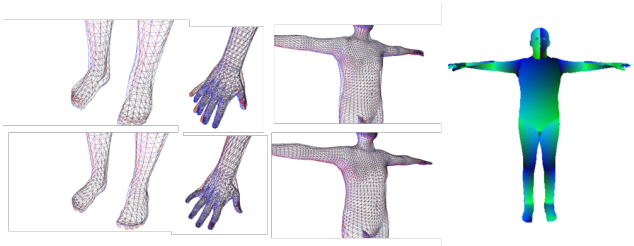

Figure 3. The Adam (blue) and SMPL (red) model before and after mesh registration. The last column is the final generated DensePose-like UVI map for Adam model

5. Dense Pose Annotation and Training

After markerless motion capture, we obtained the Adam model sequences, which are well align with the multi-view video inputs. In this step, we develop an annotation method for automatically labeling the multi-view video input to generate their corresponding UVI maps and all other information necessary for the dense pose training, based on the tracked Adam models. We train the dense pose using available DensePose architecture [18].

5.1. Building Adam-UVI Map

With the available Adam models, we need to synthesize the UVI maps as training data, given the input camera poses. We also need to take advantage of the available manually annotated UVI dataset in DensePose [18], and combine them to refrain from bias and over fitting in the training process. Moreover, it would be convenient to directly use the current DensePose framework. However, as described in Sect. 4.2, the UVI maps used in DensePose only semantically map to the SMPL model. We therefore need to have an Adam-UVI map for rendering the Adam models to UVI maps.

Our solution is to fit the Adam model to the SMPL model. To do this, we generate multiple pose examples for aligning these two models to get the average correspondence as our final fitting result. We deform the SMPL model with 64 random poses from the MoSh dataset [27], and deform the standard Adam model template to align with each SMPL model. We achieve this goal by two steps. First, we estimate a new skeleton, which is more compatible with the joints used in Adam model, using COCO+ joint regressor from[23] for each SMPL model. We then deform the Adam model to fit to each skeleton and roughly align the shape, by using the method described in Sect. 4.1, as shown in the top row of Fig. 8. We then use non-rigid ICP deformation [25] to perfectly align the Adam model with the SMPL models, see the bottom row of Fig. 8. With this alignment, the UVI map each SMPL model can be transferred to the Adam model. By averaging the 64 results, we can get the desired Adam-UVI map, as shown in the right of Fig. 8.

5.2. Building Panoptic Dense Pose Dataset

In this step, we generate the dataset for DensePose training based on the tracked Adam models and the Adam-UVI map. A complete annotation pair used in DensePose composes of 1) semantic segmentation mask, 2) segmentation polygon, 3) bounding box for each person, 4) sparse dense pose features (as u, v, i, x, y values), 5) body joints. We describe our method for getting all these components in the following.

Given the available UVI values on the Adam model vertices, it is very natural and efficient to use a standard OpenGL rendering pipeline to get annotations. By sending the per-face UVI color value, vertex positions and face indices to the OpenGL frame buffer, and setting the projection matrix based on camera matrix, we can easily get the dense UVI map for each camera view. Need to notice that here we need to use a custom OpenGL-shader to avoid the interpolation on the edge of different parts which will bring in artifacts. Since different persons share the same UVI color distribution, attention should be paid for dealing with multi-persion occlusions. By an additional uniform color coding of vertices on a person but distinct color among different persons, it is efficient to know the occlusions from the rendered color maps. The body segmentation masks, part segmentation masks can also be obtained in similar way. Bounding boxes can be computed based on the masks and the UVI maps.

Getting the 2D body joints is however not that straight forward, as there are self body part occlusions and multi-person occlusions. Actually it is also not easy to precisely mark the visible joints, because joints are located inside the human bodies and occlusions can be very complex. Here, we use a simple way to solve this problem without extra rendering. We refer to the joint regressor $\mathcal{J}^{3P\times 3M}$ used in Eqn. 3, and simply classify a joint as visible if there exists at least one visible vertex that is affected by this joint. As described, the examining of vertex visibility is very efficient by using color coding and rendering.

6. Results

In our training step, we use 30K annotations from Panoptic-Dense dataset in order to keep dataset size consistent with densepose baseline training. For testing, we use another $8K$ annotations. In each training and testing frame, there may be one or many human characters in the scene. Note we guarantee that the same person will not appear in both the training set and the testing set. The whole optimization framework is in a loop as we first perform Mocap., followed with dense pose data annotation and training. We then iterate the Mocap. again by using the newly-trained densepose detector.

In this following, we provide the quantitative and qualitative evaluation of our dense pose detector and our markerless motion capture, by comparing with the available DensePose [18] and total motion capture [22].

6.1. Panoptic Evaluation

We first present the method to evaluate the performance of dense pose detector, based on the Panoptic-Dense testing set. Because of the provided pose and viewpoint information, we can evaluate the performance in a more comprehensive way by showing the performance of dense pose detectors across viewpoints and pose clusters.

Here, our basic performance metric is the same with the one defined in DensePose [18]. For measuring a specific dense pose of a person in an UVI image, we regard the tracked Adam model as ground truth. Specifically, for each image pixel p, we back project it to the Adam model and get a vertex m_p. Also, we check the UVI value of this pixel, and find the semantic correspondence vertex m_s, according to the Adam-UVI map. We then regard the geodesic distance between m_p and m_s as the error metric for pixel p. By summing the distance error over all pixels belong to the person on an image, we can get the error for this person on an image.

Fig. 5 shows the distributions of dense pose accuracy of the original DensePose [18] (top) and our dense pose detector (middle) across viewpoints. Also, the comparison of mAP value of these two schemes on different poses are shown in the bottom. From the results, we can see that our detector substantially improve the performance on nearly all the viewpoints and poses. It can also be observed that the orignal Densepose baseline performance well in front view but the performance will drop fast in other views(side-view, back-view and top-view especially), which is hard to be annotated.(see Fig. 4)

To evaluate the dense pose consistency among difference views alone, we further measure the epipolar distances of the dense features among difference views. Specifically, for each dense pose feature on an input view, we find its semantic correspondence on the other visible views, and measure the epipolar distances. We summarize on the visible views and on all the features to get the average epipolar distance of a frame, see Fig. 6. Since the reconstruction of Adam models are not involved in this measurement, these measurements evaluate only the dense pose consistency among the views. Our dense pose detector outperforms the original baseline DensePose in this evaluation.

6.2. Quantitative Evaluation

Motion Capture Here we quantitatively evaluate our markerless capture performance by comparing with Total-Capture [22]. Table 1 shows the results for running time on each temporal frame, mean Error and standard deviation of the difference between the result models and the input hu-

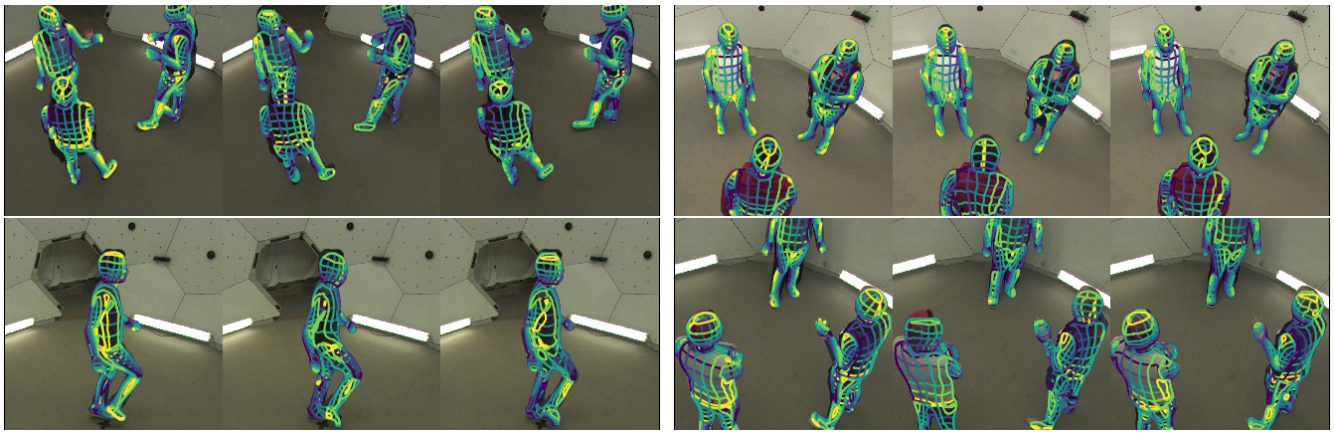

Figure 4. Example dense pose results on the Panoptic data. For each of the four examples, from left to right: the groundtruth from the multiview motion capture, DensePose baseline results [18] and our results.

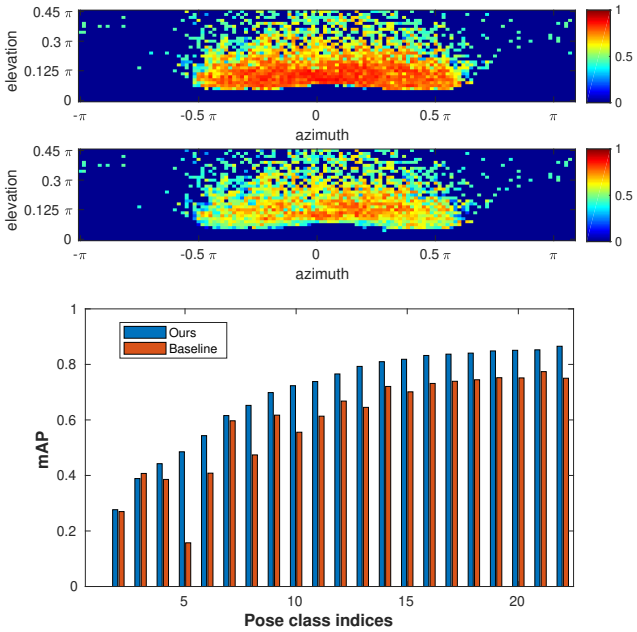

Figure 5. Dense Pose Error distribution. From top to down: error distribution of DensePose [18] over viewpoints; error distribution of our dense pose detector over viewpoints; comparison of mAP value of DensePose [18] and our dense pose detector on different pose clusters.

man silhouettes (evaluated in [22]). TotalCapture also goes with two step optimization: Joint fitting and point cloud optimization. Our methods goes with joint fitting (Sect. 4.1) and dense pose refinement (Sect. 4.2). From this comparison, we can see the refinement greatly improve the shape and pose reconstruction accuracy, and the performance is similar the the full pipeline of TotalCapture. Note that we substantially save the running time required thus make the generation of large scale Adam model-image correspondences possible. Note also that the performance of our arm

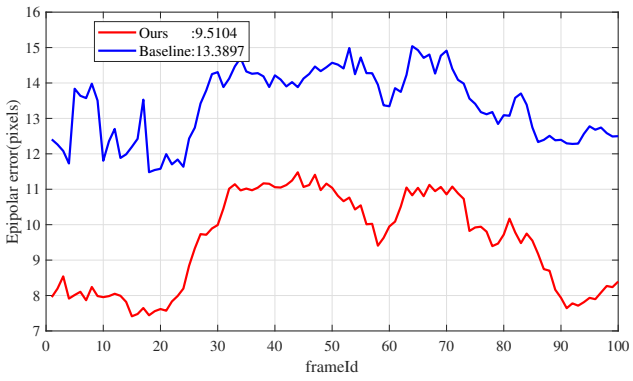

Figure 6. Epipolar distances of the dense features among difference views. See the text for detailed explanation.

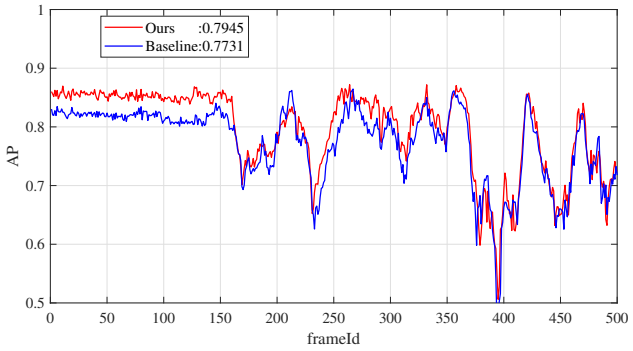

Figure 7. Quantitative evaluation using an in-the-wild video sequence from the DoubleFusion system [47]. The SMPL models estimated from [47] are regarded as groundtruth reference.

rotations is visually better than TotalCapture, which can not be quantitatively measured.

Dense Pose Detector We further quantitatively evaluate the performance of dense pose detector with different training schemes. In this experiment, we keep the training

set size and training epochs fixed but the composition different. Table 2 shows the evaluation on our Panoptic-Dense dataset. Here, "50%" dome means half of the training data are from our Panoptic data and others are from the DensePose-COCO [18], "Shuffle" means we keep the used DensePose-COCO data fixed, but will add different Panoptic-Dense training set in each epoch. "baseline-s1x" and "baseline-e2e" stand for DensePose without and with end to end training, respectively. It is reasonable that more percentage of training images from our Panoptic data, the better performance we can achieve in Panoptic-Dense testing set. Table 3 shows the evaluation on the DensePose-COCO dataset. Our result using 10% Panoptic-Dense image with shuffling outperforms other training schemes except for the $\mathbf{AP}_{50}$ measurement. As we can see from the table that that adding too much Panoptic-Dense data will lead to overfiting as the the diversity of Panoptic-Dense data background is limited which can be further improved by background augmentation [14]. Although the improvement of our training scheme is not substantial, it is still reasonable as this is measured on the human annotated dataset, which itself is not accurate enough and also that annotation of DensePose-COCO dataset if mostly from front-view(see Fig. 10. Fig. 13 compares the performance on some images from the DensePose-COCO dataset. also the AP scores can be used as a reference, it is very hard to say that high AP value means better dense pose detection performance.

To better evaluate our dense pose detector "out-side" the Panoptic-Studio [21], we use the DoubleFusion [47] system to capture per-pixel densepose annotations. In DoubleFusion, the reconstruction is conducted by simultaneously tracking of the SMPL models and fusion of the surface geometry using a single depth camera. For those successful tracking sequences, their SMPL results can be regarded as groundtruth reference. Fig. 7 shows the quantitative mparisons on DoubleFusion-Dense dataset by compareing the per-frame AP values between our dense pose detector and the original DensePose [18]. For most of the frames, the AP of our detector 0.7945 outperforms DensePose [18] with AP 0.7731. From the qualitative comparison in Fig. 12, we can see that performance of the original DensePose and ours are similar for the front views. Still, for the other challenging camera views, our results are consistently better.

Capture Dense Here we quantitative evaluate the performance of our dense pose feature based motion capture method. Fig. 8 illustrates the errors between the multiview triangulation of the dense features and their semantic correspondences on the Adam model, as described in Eqn.(5) of the main paper. Here, for each of the two results, the middle sub-figure is calculated using the original DensePose [18] method while the right one is calculated using our pose detector. Specifically, for each dense feature, we do multiview RANSAC triangulation of the same dense features on all camera views in the Panoptic studio, and get a 3D position x^m. For this dense feature, since the semantic correspondence v^m on the Adam model is available, We can plot the distance errors between x^m and v^m on the Adam models. Also, in Fig. 9, we compare the quantitative distance errors over time using a sequence containing multiple temporal frames. From the figures, we can see that after data training using our dense pose dataset, the dense pose consistency among difference views is improved and the semantic alignment with the Adam model becomes better.

Fig. 11 illustrates the motion capture performance as well as the dense pose performance on two of the Panoptic-Studio Dataset frames. By adding the dense features as regularizer for motion capture refinement, we improve the capture performance. For example, the tracking of the hip part is clearly improved. This is mainly due to the skeleton detection approach [9] on the hip joints are usually error-pone while dense features can help to align them better.

7. Conclusion

In this paper, we have tentatively explored the scientific relationship between dense human parsing (dense pose estimation) and multiview human reconstruction. We have developed a new markerless motion capture algorithm based on dense pose estimation, as well as improving the performance of dense pose detector based on the multiview images with its high quality markerless motion capture results. We have also made them in-a-loop, and show advantage of such iteration optimization mechanism.

Overall, from the historical aspect, markerless motion capture has been explored for about 30 years, but it is still not popular for real applications. One of the main obstacles is the real-time performance, which has been mostly solved by the recent advancement of the real-time and robust 2D sparse human detector. Another obstacle is the accuracy, which is by far less than the marker based ones. We hope that by using the 2D dense parsing technique like dense pose, accuracy will be substantially improved in the near future. Actually, we have demonstrated some of the corner cases and shown our superior performance over the state-of-the-art. Moreover, our proposed iterative deep learning framework takes advantages of the large amount of dense multi-view information, and essentially, it encodes the multi-view information and knowledge into a single dense pose detector. We believe that the performance improved dense pose detector can be used in interesting tasks such as single image human body reconstruction. We also believe that our idea of combining dense pose and multiview markerless motion capture can inspire many future researches like stereo matching and 3D reconstruction on human body.

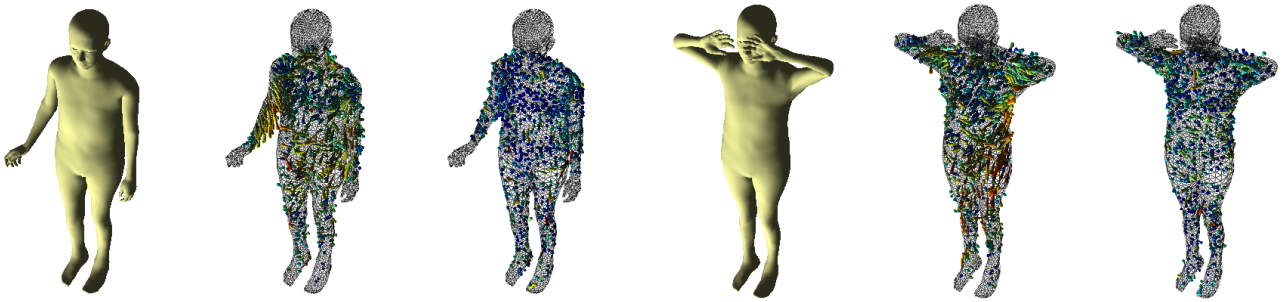

Figure 8. The plots of distance errors between the multiview triangulation of the dense features and their semantic correspondences on the Adam model. For each of the two cases, the left sub-figure is the tracked Adam model. The middle sub-figure is the distance plot using the original DensePose baseline, and the right one is the distance plot obtained by our dense pose detector. The length and the color of arrows on the model encodes the magnitude of the error. Red is lager while blur is smaller.

Scheme	**AP**	**AP**$_{50}$	**AP**$_{75}$	**AP**$_M$	**AP**$_L$	**AR**	**AR**$_{50}$	**AP**$_{75}$	**AR**$_M$	**AR**$_L$
10% dome-Shuffle	0.7102	0.9747	0.9198	0.2960	0.7207	0.7498	0.9801	0.9338	0.3537	0.7607
20% dome	0.7057	0.9772	0.9108	0.3306	0.7167	0.7436	0.9801	0.9289	0.3611	0.7540
50% dome	0.7296	0.9794	0.9320	0.3825	0.7378	0.7661	0.9854	0.9444	**0.4574**	0.7749
100% dome	**0.7463**	**0.9795**	**0.9443**	**0.3841**	**0.7565**	**0.7811**	**0.9862**	**0.9517**	0.4537	**0.7904**
baseline-s1x	0.5660	0.9449	0.6588	0.0188	0.5808	0.6106	0.9529	0.7328	0.0259	0.6255
baseline-e2e	0.5617	0.9358	0.6405	0.0162	0.5764	0.6108	0.9497	0.7276	0.0352	0.6256

Table 2. Per-instance evaluation of DensePose-RCNN performance on Panoptic-Dense testing set.

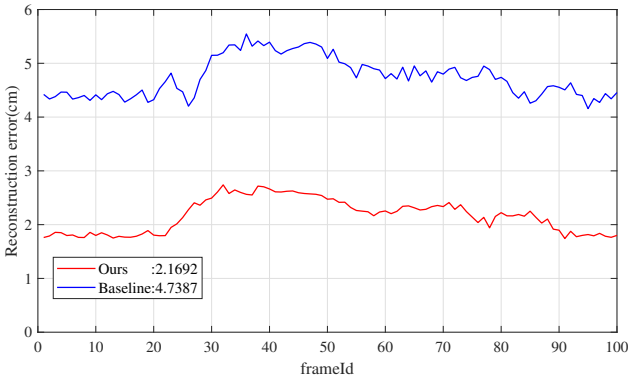

Figure 9. Multi-view consistency evaluation using our Panoptic dense pose data. The curves give the per-frame average distance error between the multiview triangulated dense features and the semantic correspondences on the Adam model.

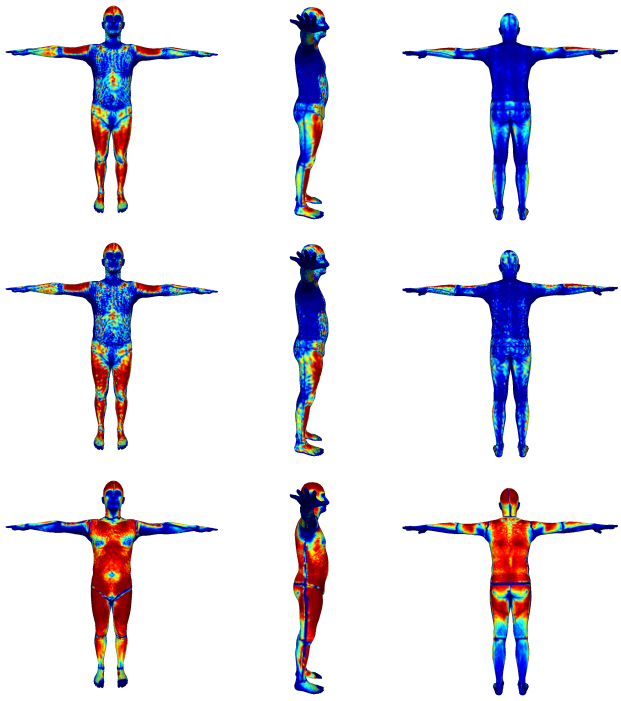

Figure 10. Visualization of the dense feature distributions. From top to bottom: DensePose-COCO training set, DensePose-COCO validation set and our Panoptic-Dense training set. Red means higher frequency while blue means lower frequency.

References

[1] Realitycapture software. www.capturingreality.com/. 3

[2] Openpose library. https://github.com/CMU-Perceptual-Computing-Lab/openpose, 2013. 1, 3, 4

[3] T. Alldieck, M. A. Magnor, W. Xu, C. Theobalt, and G. Pons-Moll. Video based reconstruction of 3d people models. 2018. 1

[4] A. O. Balan, L. Sigal, M. J. Black, J. E. Davis, and H. W. Haussecker. Detailed human shape and pose from images.

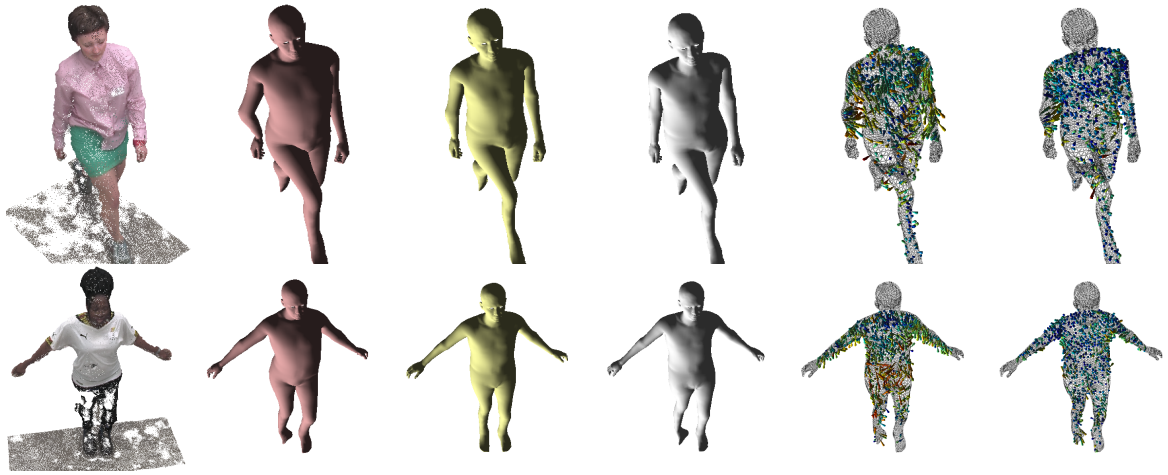

Figure 11. Qualitative Mocap and dense pose comparison. From left to right: reconstructed point-cloud used in TotalCapture [22], our motion capture result using joint fitting only, our motion capture result after dense pose refinement, motion capture result in TotalCapture, triangulated errors of the dense features using the baseline DensePose, and the triangulated errors of the dense features based on our dense pose detector.

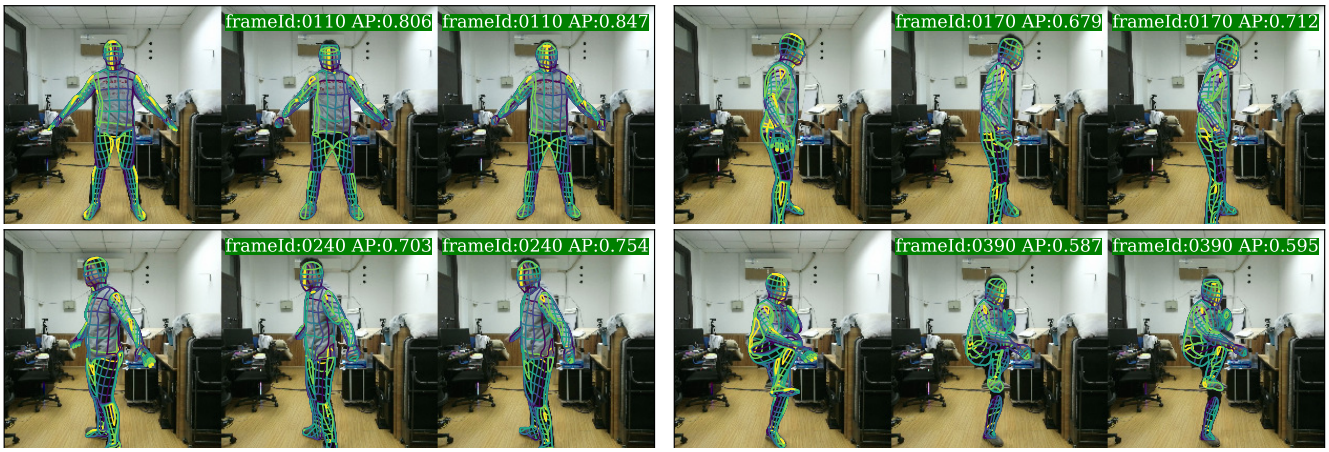

Figure 12. Example results for the in-the-wild data using a DoubleFusion [47] sequence. For each of the four examples, from left to right : DoubleFusion [47] results, DensePose baseline results[18], and our results.

In *2007 IEEE Computer Society Conference on Computer Vision and Pattern Recognition (CVPR 2007), 18-23 June 2007, Minneapolis, Minnesota, USA*, 2007. 1

[5] V. Belagiannis, S. Amin, M. Andriluka, B. Schiele, N. Navab, and S. Ilic. 3d pictorial structures for multiple human pose estimation. In *2014 IEEE Conference on Computer Vision and Pattern Recognition, CVPR 2014, Columbus, OH, USA, June 23-28, 2014*, pages 1669–1676, 2014. 3

[6] F. Bogo, M. J. Black, M. Loper, and J. Romero. Detailed full-body reconstructions of moving people from monocular RGB-D sequences. In *2015 IEEE International Conference on Computer Vision, ICCV 2015, Santiago, Chile, December 7-13, 2015*, pages 2300–2308, 2015. 1, 2

[7] F. Bogo, A. Kanazawa, C. Lassner, P. Gehler, J. Romero, and M. J. Black. Keep it smpl: Automatic estimation of 3d human pose and shape from a single image. In *European Conference on Computer Vision*, pages 561–578. Springer, 2016. 1, 3, 4

[8] C. Bregler, J. Malik, and K. Pullen. Twist based acquisition and tracking of animal and human kinematics. *International Journal of Computer Vision*, 56(3):179–194, 2004. 2

[9] Z. Cao, T. Simon, S.-E. Wei, and Y. Sheikh. Realtime multi-person 2d pose estimation using part affinity fields. In *CVPR*, 2016. 1, 3, 8

[10] G. K. M. Cheung, S. Baker, and T. Kanade. Shape-from-silhouette across time part I: theory and algorithms. *International Journal of Computer Vision*, 62(3):221–247, 2004. 2

[11] A. Collet, M. Chuang, P. Sweeney, D. Gillett, D. Evseev, D. Calabrese, H. Hoppe, A. Kirk, and S. Sullivan. High-quality streamable free-viewpoint video. *ACM Transactions on Graphics (TOG)*, 34(4):69, 2015. 1

[12] S. Corazza, L. Mündermann, E. Gambaretto, G. Ferrigno,

Figure 13. Example results from the DensePose-COCO dataset. From left to right: groundtruth, results [18] and our results. It's hard to tell that higher AP values reflects better results. In the second example, visually the second resuls is more tidy (especially the side part) however the AP value is lower. In the third results, it's hard to use this AP value to tell the one instance is better then another.

and T. P. Andriacchi. Markerless motion capture through visual hull, articulated ICP and subject specific model generation. *International Journal of Computer Vision*, 87(1-2):156–169, 2010. 2

[13] M. Dou, S. Khamis, Y. Degtyarev, P. Davidson, S. R. Fanello, A. Kowdle, S. O. Escolano, C. Rhemann, D. Kim, J. Taylor, et al. Fusion4d: real-time performance capture of challenging scenes. *ACM Transactions on Graphics (TOG)*, 35(4):114, 2016. 1

[14] D. Dwibedi, I. Misra, and M. Hebert. Cut, Paste and Learn: Surprisingly Easy Synthesis for Instance Detection. In *ICCV*, 2017. 8

[15] A. Elhayek, E. de Aguiar, A. Jain, J. Tompson, L. Pishchulin, M. Andriluka, C. Bregler, B. Schiele, and C. Theobalt. Efficient convnet-based marker-less motion capture in general scenes with a low number of cameras. In *IEEE Conference on Computer Vision and Pattern Recognition, CVPR 2015, Boston, MA, USA, June 7-12, 2015*, pages 3810–3818, 2015.

Scheme	**AP**	**AP**$_{50}$	**AP**$_{75}$	**AP**$_M$	**AP**$_L$	**AR**	**AR**$_{50}$	**AP**$_{75}$	**AR**$_M$	**AR**$_L$
10% dome-Shuffle	**0.5019**	0.8420	**0.5182**	**0.4401**	**0.5099**	**0.5855**	**0.9050**	**0.6326**	**0.4624**	**0.5937**
20% dome	0.4699	0.8435	0.4824	0.4168	0.4886	0.5626	0.9050	0.6014	0.4411	0.5708
50% dome	0.4442	0.8235	0.4344	0.3894	0.4624	0.5383	0.8917	0.5644	0.4234	0.5461
100% dome	0.0296	0.1174	0.0032	0.0174	0.0316	0.0717	0.2465	0.0214	0.0191	0.0753
baseline-s1x	0.4748	0.8368	0.4820	0.4262	0.4948	0.5748	0.9041	0.6144	0.4496	0.5832
baseline-e2e	0.4883	**0.8481**	0.5100	0.4223	0.5051	0.5782	0.9028	0.6237	0.4546	0.5865

Table 3. Per-instance evaluation of DensePose-RCNN performance on COCO-Dense `minival` subset.

3

[16] V. Ganapathi, C. Plagemann, D. Koller, and S. Thrun. Real time motion capture using a single time-of-flight camera. In *The Twenty-Third IEEE Conference on Computer Vision and Pattern Recognition, CVPR 2010, San Francisco, CA, USA, 13-18 June 2010*, pages 755–762, 2010. 3

[17] D. Gavrila and L. S. Davis. 3-d model-based tracking of humans in action: a multi-view approach. In *1996 Conference on Computer Vision and Pattern Recognition (CVPR '96), June 18-20, 1996 San Francisco, CA, USA*, pages 73–80, 1996. 2

[18] R. A. Güler, N. Neverova, and I. Kokkinos. Densepose: Dense human pose estimation in the wild. In *CVPR*, 2018. 1, 2, 3, 5, 6, 7, 8, 10, 11

[19] R. A. Güler, G. Trigeorgis, E. Antonakos, P. Snape, S. Zafeiriou, and I. Kokkinos. Densereg: Fully convolutional dense shape regression in-the-wild. In *CVPR*, volume 2, page 5, 2017. 1, 3

[20] A. Harltey and A. Zisserman. *Multiple view geometry in computer vision (2. ed.)*. Cambridge University Press, 2006. 5

[21] H. Joo, H. Liu, L. Tan, L. Gui, B. Nabbe, I. Matthews, T. Kanade, S. Nobuhara, and Y. Sheikh. Panoptic studio: A massively multiview system for social motion capture. In *Proceedings of the IEEE International Conference on Computer Vision*, pages 3334–3342, 2015. 3, 4, 8

[22] H. Joo, T. Simon, and Y. Sheikh. Total capture: A 3d deformation model for tracking faces, hands, and bodies. In *CVPR*, 2018. 1, 2, 3, 4, 6, 7, 10

[23] A. Kanazawa, M. J. Black, D. W. Jacobs, and J. Malik. End-to-end recovery of human shape and pose. In *Computer Vision and Pattern Regognition (CVPR)*, 2018. 1, 3, 5

[24] R. Kehl and L. J. V. Gool. Markerless tracking of complex human motions from multiple views. *Computer Vision and Image Understanding*, 104(2-3):190–209, 2006. 2

[25] H. Li, B. Adams, L. J. Guibas, and M. Pauly. Robust single-view geometry and motion reconstruction. *ACM Trans. Graph.*, 28(5):175:1–175:10, 2009. 5

[26] Y. Liu, J. Gall, C. Stoll, Q. Dai, H.-P. Seidel, and C. Theobalt. Markerless motion capture of multiple characters using multiview image segmentation. *IEEE transactions on pattern analysis and machine intelligence*, 35(11):2720–2735, 2013. 1, 2, 4

[27] M. Loper, N. Mahmood, and M. J. Black. Mosh: Motion and shape capture from sparse markers. *ACM Transactions on Graphics (TOG)*, 33(6):220, 2014. 1, 5

[28] M. Loper, N. Mahmood, J. Romero, G. Pons-Moll, and M. J. Black. Smpl: A skinned multi-person linear model. *ACM Transactions on Graphics (TOG)*, 34(6):248, 2015. 2, 3, 4

[29] J. Martinez, R. Hossain, J. Romero, and J. J. Little. A simple yet effective baseline for 3d human pose estimation. In *IEEE International Conference on Computer Vision, ICCV 2017, Venice, Italy, October 22-29, 2017*, pages 2659–2668, 2017. 1, 3

[30] D. Mehta, S. Sridhar, O. Sotnychenko, H. Rhodin, M. Shafiei, H. Seidel, W. Xu, D. Casas, and C. Theobalt. Vnect: real-time 3d human pose estimation with a single RGB camera. *ACM Trans. Graph.*, 36(4):44:1–44:14, 2017. 1, 3

[31] N. Neverova, R. A. Güler, and I. Kokkinos. Dense pose transfer. In *Computer Vision - ECCV 2018 - 15th European Conference, Munich, Germany, September 8-14, 2018, Proceedings, Part III*, pages 128–143, 2018. 1

[32] A. Newell, K. Yang, and J. Deng. Stacked hourglass networks for human pose estimation. In *Computer Vision - ECCV 2016 - 14th European Conference, Amsterdam, The Netherlands, October 11-14, 2016, Proceedings, Part VIII*, pages 483–499, 2016. 3

[33] L. Pishchulin, E. Insafutdinov, S. Tang, B. Andres, M. Andriluka, P. V. Gehler, and B. Schiele. Deepcut: Joint subset partition and labeling for multi person pose estimation. In *2016 IEEE Conference on Computer Vision and Pattern Recognition, CVPR 2016, Las Vegas, NV, USA, June 27-30, 2016*, pages 4929–4937, 2016. 1

[34] G. Pons-Moll, S. Pujades, S. Hu, and M. Black. ClothCap: Seamless 4D clothing capture and retargeting. *ACM Transactions on Graphics, (Proc. SIGGRAPH)*, 36(4), 2017. 1

[35] G. Pons-Moll, S. Pujades, S. Hu, and M. J. Black. Clothcap: seamless 4d clothing capture and retargeting. *ACM Trans. Graph.*, 36(4):73:1–73:15, 2017. 3

[36] G. Pons-Moll, J. Romero, N. Mahmood, and M. J. Black. Dyna: a model of dynamic human shape in motion. *ACM Trans. Graph.*, 34(4):120:1–120:14, 2015. 2

[37] J. Romero, D. Tzionas, and M. J. Black. Embodied hands: Modeling and capturing hands and bodies together. *ACM Transactions on Graphics (TOG)*, 36(6):245, 2017. 3, 4

[38] J. Shotton, A. W. Fitzgibbon, M. Cook, T. Sharp, M. Finocchio, R. Moore, A. Kipman, and A. Blake. Real-time human pose recognition in parts from single depth images. In *The 24th IEEE Conference on Computer Vision and Pattern Recognition, CVPR 2011, Colorado Springs, CO, USA, 20-25 June 2011*, pages 1297–1304, 2011. 3

[39] T. Simon, H. Joo, I. A. Matthews, and Y. Sheikh. Hand keypoint detection in single images using multiview bootstrapping. In *2017 IEEE Conference on Computer Vision and Pattern Recognition, CVPR 2017, Honolulu, HI, USA, July 21-26, 2017*, pages 4645–4653, 2017. 3

[40] C. Stoll, N. Hasler, J. Gall, H. Seidel, and C. Theobalt. Fast articulated motion tracking using a sums of gaussians body model. In *IEEE International Conference on Computer Vision, ICCV 2011, Barcelona, Spain, November 6-13, 2011*, pages 951–958, 2011. 2

[41] D. Tomè, C. Russell, and L. Agapito. Lifting from the deep: Convolutional 3d pose estimation from a single image. In *2017 IEEE Conference on Computer Vision and Pattern Recognition, CVPR 2017, Honolulu, HI, USA, July 21-26, 2017*, pages 5689–5698, 2017. 1, 3

[42] D. Vlasic, I. Baran, W. Matusik, and J. Popovic. Articulated mesh animation from multi-view silhouettes. *ACM Trans. Graph.*, 27(3):97:1–97:9, 2008. 2

[43] S. Wei, V. Ramakrishna, T. Kanade, and Y. Sheikh. Convolutional pose machines. In *2016 IEEE Conference on Computer Vision and Pattern Recognition, CVPR 2016, Las Vegas, NV, USA, June 27-30, 2016*, pages 4724–4732, 2016. 1, 3

[44] X. K. Wei, P. Zhang, and J. Chai. Accurate realtime full-body motion capture using a single depth camera. *ACM Trans. Graph.*, 31, 2012. 3

[45] W. Xu, A. Chatterjee, M. Zollhöfer, H. Rhodin, D. Mehta, H. Seidel, and C. Theobalt. Monoperfcap: Human performance capture from monocular video. *ACM Trans. Graph.*, 37(2):27:1–27:15, 2018. 3

[46] G. Ye, Y. Liu, N. Hasler, X. Ji, Q. Dai, and C. Theobalt. Performance capture of interacting characters with handheld kinects. In *Computer Vision - ECCV 2012 - 12th European Conference on Computer Vision, Florence, Italy, October 7-13, 2012, Proceedings, Part II*, pages 828–841, 2012. 2

[47] T. Yu, Z. Zheng, K. Guo, J. Zhao, Q. Dai, H. Li, G. Pons-Moll, and Y. Liu. Doublefusion: Real-time capture of human performances with inner body shapes from a single depth sensor. In *CVPR*, 2018. 1, 2, 3, 7, 8, 10

[48] Z. Zhang. Iterative closest point (ICP). In *Computer Vision, A Reference Guide*, pages 433–434. 2014. 2